EXPLORATION OF THE FEASIBILITY OF ADAPTIVE SPHERICAL NEAR-FIELD ANTENNA MEASUREMENTS

Vincent Beaulé, Derek McNamara
EECS, University of Ottawa, 800 King Edward Avenue
Ottawa, Ontario K1N 6N5, Canada

Daniël Janse van Rensburg
Nearfield Systems Inc.
19730 Magellan Drive
Torrance, CA 90502-1104, USA

Leili Shafai & Shantnu Mishra
DFL, Canadian Space Agency
3701 Carling Avenue
Kanata, Ontario K2H 8S2, Canada

ABSTRACT

The feasibility of using adaptive acquisition techniques to reduce the overall testing time in spherical near-field (SNF) antenna measurements is investigated. The adaptive approach is based on the premise that near-field to far-field (NF-FF) transformation time is small compared to data acquisition time, so that such computations can be done repeatedly while data is being acquired. This allows us to use the transformed FF data to continuously compute and monitor pre-defined decision functions (formed from the antenna specifications most important to the particular AUT) while data is being acquired. We do not proceed with a complete scan of the measurement sphere but effectively allow the probe to follow a directed path under control of an acquisition rule, so that the sampled NF datapoints constitute an acquisition map on the sphere (the geographical allusion being purposeful). SNF data acquisition can be terminated based on decision function values, allowing the smallest amount of data needed to ensure accurate determination of the AUT performance measures. We demonstrate the approach using actual NF data for several decision functions and acquisition rules.

1. Introduction

The use of adaptive acquisition techniques to reduce the overall testing time in planar near-field antenna measurements was investigated in [1]. The feasibility of a similar approach in spherical near-field (SNF) measurements, slightly more involved than its planar counterpart, is explored in this paper. As the antenna under test (AUT) becomes electrically larger, the number of spatial samples over the measurement sphere required to properly predict the far-field increases [2], and so does the time needed for the acquisition. It is understood that the acquisition time is dominated by the mechanical movement of the probe and the electronics used to sample the near-field. (We refer to movement of the probe even though in many SNF acquisition systems the probe is actually stationary and the AUT is moved). In this work it's assumed that the time taken to perform the near-field to far-field (NF-to-FF) transformation, and the computation of AUT performance parameters from this FF data, is small compared to the NF data acquisition time. This is certainly true with all commercial SNF systems. Therefore, the NF-to-FF transformation can be done repeatedly without noticeably impacting the total test time duration. It is then possible to monitor the evolution of AUT performance parameters as the NF data is being acquired, and once these have been determined with sufficient accuracy one can halt acquisition. The driving idea behind adaptive acquisition is to enable measurements that use just the required number of NF data samples – no more, no less - for the required accuracy in the AUT performance parameters of interest. In this paper the feasibility of adaptive SNF antenna measurement is studied as a means of reducing the overall acquisition time.

2. Conventional Partial Scan Methods

The electromagnetic theory upon which the near-field measurement techniques are based requires the measurement surface to fully enclose the AUT. In the SNF case this surface is the complete measurement sphere, which is indeed closed. Hence there is no inherent truncation present for SNF measurements.

A given AUT has a minimum radius sphere that completely encloses it. Spherical wave expansion (SWE) theory can be used to show that as the minimum sphere gets larger so does the number (N) of spherical modes needed to represent the field [2]. As the number of significant modes N increases, the sampling density required to reconstruct the fields without mode aliasing increases since the required angular increments between samples on the measurement sphere are $\Delta\theta = \Delta\phi = 2\pi/(2N+1)$. As seen, with a larger minimum sphere, the step in θ and φ becomes smaller and a large number of field samples must be acquired, leading to an increase in data acquisition time. Electrically large antennas are usually highly directive – most of the energy is concentrated in a cluster of directions in space. In such a case it is possible to limit the acquisition of NF data to only that portion of the measurement sphere subtended by these directions, with the field outside the sampled portions on the measurement sphere assumed to be zero. This deliberate truncation certainly reduces the number of samples that need to be acquired, and hence the acquisition time. However, such a truncation introduces a non-physical discontinuity in the NF data over the measurement sphere. Such a discontinuity produces some undesirable effects in the FF pattern obtained from transformation of the truncated NF data (the so-called truncation error).

Conventionally, the above-mentioned partial scan of the measurement sphere is accomplished by selecting a spherical polar cap defined by an angle from the centre of the measurement sphere – the truncation angle (θ_t) indicated in Fig.1. The cap must be selected to be in the same direction as the expected far-field pattern maximum so that the cap captures most of the power emanating from the AUT. With such a correctly located spherical cap of sufficiently large size it is possible to define the validity angle (θ_v), which is the angle out to which the FF pattern derived from the truncated NF set coincides sufficiently well with what would have been obtained if a full-sphere acquisition had been performed. The validity angle is usually narrower than the truncation angle. It can be determined geometrically using the sketch in Fig.1 to be

$$\theta_v = \theta_t - \theta_{tf} = \theta_t - \sin^{-1}(r_o / r_{sph}) \qquad (2.1)$$

where r_0 is the radius of the minimum sphere enclosing the AUT and r_{sph} is the radius of the measurement sphere. The notation used in (2.1) is similar to that in [3]. We call the above partial scan the conventional one.

A few authors, for example [3,4], have proposed techniques that can be used to reduce the effects of truncation in SNF measurements when SNF data is acquired on a polar cap of pre-determined angle. The algorithm by Martini et al. [4] consists of iteratively imposing matching of the back-computed NF on the measurement sphere with the actual measured NF samples there, and performing spectral filtering in the SWE mode domain based on a knowledge of which SWE modes will be significant for the AUT of known physical extent. Although truncation reduction techniques have not yet gained widespread acceptance as a mainstream solution in industry, the work in [4] will be applicable to the adaptive approach being to be discussed in Section 3 if the algorithm can be executed sufficiently fast.

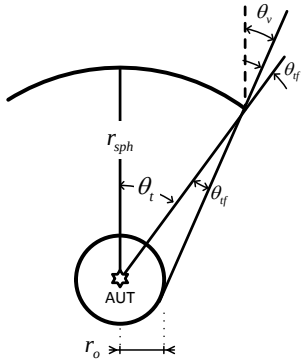

Figure 1 - Conventional Truncation Geometry of SNF Measurement Sphere

3. Proposed Adaptive SNF Algorithm

Acquisition rules are used to iteratively acquire the samples on the measurement sphere. An acquisition rule refers to the algorithm that guides the probe path on the measurement sphere. The result of the application of an acquisition rule is an acquisition map of points on the measurement sphere where the NF data is actually acquired. The acquisition rules are based on the assumption that the NF sample points with the highest electrical field amplitude are the most valuable in achieving fast convergence of parameters of interest (directivity, sidelobe levels and FF pattern). From the n-th to the (n+1)-th iteration the acquisition rule adapts itself based on previously acquired NF data samples, and so shapes the acquisition map as the acquisition process proceeds. The acquisition map is thus a shaped partial scan rather than a simple spherical cap referred to as the "conventional partial scan" in Section 2. While such acquisition is proceeding NF-to-FF transformation of the NF data is performed continually, and the relevant AUT performance parameters are computed. Once the parameters have converged in a manner that satisfies an appropriately-defined set of decision functions the acquisition is halted. In this paper we will for the purposes of discussion demonstrate the use of just two acquisition rules. In devising these we made the assumption that a dual-polarized probe is being used,

allowing us to sample two orthogonal field components tangential to the measurement sphere at each NF data sample point. Also, in each of these rules the starting data point is currently at a pole of the measurement sphere. In practice this would be a severe limitation, because in reality the region of highest electric field magnitude is of most value and should be acquired first. More sophisticated acquisition rules will assume some *a priori* knowledge about the AUT (eg. the approximate direction of the maximum fields; its physical size) and start at the appropriate location on the measurement sphere. With every movement of the probe an acquisition rule must sample an additional NF data point to reduce time wasted on mechanical motion without data acquisition. Sampling redundancy, if any, must be minimal.

3.1 Acquisition Rules

The ***first acquisition rule*** results in an acquisition map (illustrated in Fig.2) that is the same as that of the conventional partial scan method. In other words, the rule results in a growing cap of sample points, with scanning in ϕ. The truncation angle θ_t is increased after each iteration by an amount $\Delta\theta$. Note the first iteration has $\theta = 0°$ and the probe completes a 360° rotation about the z-axis. The second iteration has $\theta = \Delta\theta°$ and the probe again completes a 360° rotation. The first acquisition rule is used as a baseline to compare the other. The n-th iteration encompasses the sampling points of all previous iterations. The ***second acquisition rule*** is a two-fold process. The *first iteration* of this rule proceeds as follows : The probe starts at $\theta = \phi = 0°$, and then scans in θ until a sampling point is reached where the total measured electrical field amplitude

$$\left|\bar{E}_{NF}\right| = \sqrt{\left|E_{NF\theta}\right|^2 + \left|E_{NF\phi}\right|^2} \qquad (3.1)$$

is less than a pre-defined threshold value. The probe then increments its position by $\Delta\phi$ and comes back to centre of the measurement sphere to increment again its position by $\Delta\phi$. These steps are repeated until ϕ has gone from 0 to 360°. The **second and subsequent iterations** of this rule then proceed as follows: Each iteration adds NF data acquired at all sample points lying within a user-defined band of width $m\Delta\theta$ circumscribing the acquisition map created during the previous iteration. Integer *m* sets the width of this band. while following the acquisition map created during the previous iteration. This process will favour particular regions of higher electric field magnitude and therefore allow for a level of adaptation as the process evolves. The described process is illustrated in Fig.3. Note that no sample point is missed between iterations.

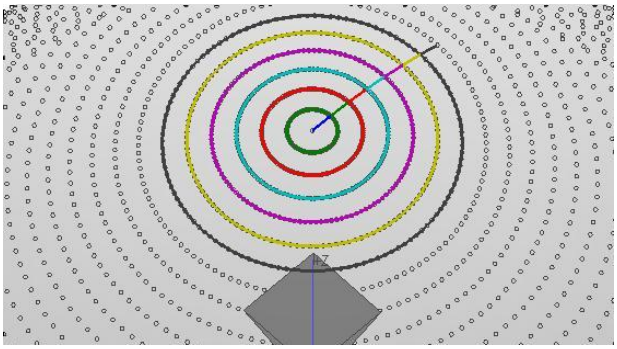

Figure 2 - Acquisition map obtained using the first acquisition rule considered in the paper, after seven iterations. NF points on the measurement sphere are denoted by the ○ symbols. The acquisition map is the set of circles shown, each colour representing those points sampled during a different iteration.

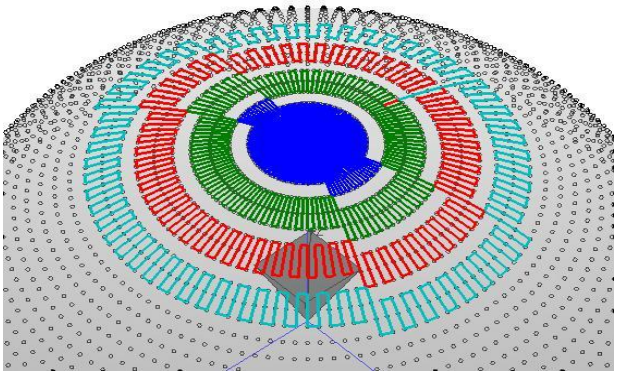

Figure 3 - Acquisition map obtained using the second acquisition rule considered in the paper, after four iterations. NF points on the measurement sphere are denoted by the ○ symbols. The acquisition map consists of the set of loci shown, each colour representing those points sampled during a different iteration. A horn AUT is shown at the sphere centre.

3.2 Decision Functions

As the NF datapoints are being computed (it need not only be the end of an iteration) the NF-to-FF transformation is executed and the values of a set of decision functions (based on the resulting FF values) is computed to decide if the acquisition process must continue or stop. The decision must be unambiguous, and thus decision functions are best related in some way to the AUT performance parameters of interest. As for the acquisition rules, we consider just three possible decision functions here for discussion purposes. In the experimental results to be shown in Section 5 we will plot decision function values at the end of each iteration only, and so these functions will be defined in such terms.

The *first decision function* is simply the directivity value $D_{co}^{n}(\theta_i,\phi_j)$ at the end of the n-th iteration, where (θ_i,ϕ_j) is the direction in which the directivity is being monitored (eg. the direction in which the directivity is a maximum). The *second decision function* is the change of co-polar directivity between the n-th and (n-1)-th . As the directivity reaches its final value – that is, the value that would be obtained by acquiring NF data for the AUT on the complete measurement sphere – its derivative tends towards zero. Thus the second decision function considered in this paper will be the directivity difference function

$$\Delta D_{co}^{n}(\theta_i,\phi_j)=10\log D_{co}^{n}(\theta_i,\phi_j)-10\log D_{co}^{n-1}(\theta_i,\phi_j) \quad (3.2)$$

When the change in directivity reaches a value close to zero, less than 0.1dB say (the desired accuracy for the measured directivity), the acquisition stops if all other decision functions needed have also "converged". The *third decision function* involves the difference in FF patterns between iterations. An error term in direction (θ_i,φ_i) after the n-th iteration is determined from the co-polarized electric field $E_{co}^{n}\left(\theta_i,\phi_j\right)$ and $E_{co}^{n-1}\left(\theta_i,\phi_j\right)$ as

$$f_{co}^{n}\left(\theta_i,\phi_j\right)=\frac{\left|E_{co}^{n}\left(\theta_i,\phi_j\right)\right|-\left|E_{co}^{n-1}\left(\theta_i,\phi_j\right)\right|}{\max\limits_{i,j}\left\{\left|E_{co}^{n}\left(\theta_i,\phi_j\right)\right|\right\}} \quad (3.3)$$

Such an error term in a particular direction (θ_i,ϕ_j), or set of directions, can be used to define a decision function. Acquisition stops when this and all other selected decision functions have reached their specified threshold values.

4. Tools Developed to Simulate the SNF Adaptive Algorithm

In order to study the SNF adaptive algorithms some customized tools are necessary. We use the NSI2000 software from Nearfield Systems Inc. [5] to access the NF data and perform the NF-to-FF transformation. All other processing is done using the Matlab [6] environment due to its flexibility, and the ready access to numerical analysis and other routines that it provides. Thus the adaptive algorithm is implemented in Matlab. The Matlab *object linking and embedding* (OLE) feature [6] is used to create a Matlab *instance* from NSI2000. This capability allows NSI2000 to transfer matrices to and from Matlab and use Matlab to run custom scripts. Matlab script based animations were also developed as a visual aid for the adaptive SNF study. Figures 2 and Figure 3 that were referred to earlier are examples of the visualisations produced by the animation scripts. It provides an easy way to appreciate the actual probe movement. Such a tool can be combined with the acquisition software to visualize the evolution of the acquisition map during actual measurement. Access to Matlab toolboxes [6] is particularly useful. For example, the Matlab function *imdilate* (part of the Image Processing Toolbox) can be configured to find local maxima in an image. It extremely rapid, as it is intended for real-time computer vision applications. Thus it can be used in the adaptive algorithm to rapidly locate sidelobe peaks between iterations (an important performance parameter), and these values in turn used in decision functions like (3.3).

5. Experimental Results from NF Datasets

With the suggested technique and the tools devised, the adaptive algorithm is here applied to a few NF datasets. Such datasets were obtained from actual antenna measurements, and so including the noise, mechanical vibrations, and other problems inherent in real-world measurements. In this study we use datasets acquired over complete measurement spheres, and then emulate the acquisition of adaptive acquisition maps in software by selecting the datapoints picked by the acquisition rule. In practice the complete sphere datasets would not actually be acquired, and only those points identified by the acquisition map as the algorithm progresses would be sampled. Information on the three AUTs used is provided in Table 1.

Table 1 - AUTs considered for decision function assessment. Pattern maximum points towards a pole in the case of the SGH and FPA, but not for the DIP.

Antenna Designation	*Type*	*AUT Size*	*Directivity*
SGH	Standard Gain Horn	$3.9\lambda\times5.3\lambda$	21.6 dBi
FPA	Flat Panel Array	$21.4\lambda\times21.4\lambda$	30.5 dBi
DIP	Dipole	0.5λ	3.9 dBi

5.1 Demonstration of Decision Function Examples

Using the first acquisition rule, observation of the co-polarized directivity as the acquisition map increases in size yields the results in Fig.4, and the related Fig.5 where a three-point running average of $\Delta D_{co}^{n}(\theta_i,\phi_j)$ in (3.2) is shown, for the three AUTs. In both cases direction (θ_i,ϕ_j) is selected to be that of the pattern maximum. This data shows that the change in directivity

for all three antenna cases converges to zero as the measurement surface approaches the full sphere. Convergence is quicker for the highest gain FPA and slowest for the DIP, as one would expect. A threshold for such a decision function would be related to the expected accuracy with which directivity can be measured. The third decision function demonstrated uses the normalized error term in (3.3), and searches over all directions (θ_i, ϕ_j) on the radiation sphere for its largest value. Thus Fig.6 shows $\max_{i,j}\left\{20\log\left|f_{co}^{n}(\theta_i,\phi_j)\right|\right\}$ for each of the three AUTs. A threshold value for such a decision function might be -40dB. Although relatively well-behaved in this instance, such a decision function could be misleading. We might end up sampling the radiation pattern at a deep null, where changes from one computation of the decision function to the next might be large, in spite of the fact that other pattern points of real interest might already have settled down. In such a case it would be better to select sets of specific directions (θ_i, ϕ_j), such as the main lobe and sidelobe maxima, and observe quantity (3.3) there. Fig.7 shows the first decision function, namely directivity, in three different directions (θ_i, ϕ_j), namely that of the three highest sidelobes on the radiation sphere. These directions are located using the function mentioned at the end of Section 4. It is apparent from Figs. 4 through 7 that, in the case of the SGH and FPA, much less than 50% of the measurement sphere needs to be scanned to achieve reliable pattern information, even for the simple conventional partial scan map (that is, first acquisition rule). This fact is already known to SNF practitioners. What we are showing here is that by monitoring the values of appropriate decision functions it is possible to judge whether acquisition can be terminated. It is of course also possible to display the evolution of the AUT radiation pattern as the adaptive algorithm proceeds. For example, Fig.8 shows the pattern of the SGH after eight iterations using the second acquisiton rule. We here show it compared to the full sphere result; in practice we would compare the patterns from iteration to iteration since the full sphere case would not be available. Finally, note that we have purposefully also shown the results for the dipole (DIP), which is an example of an AUT where the adaptive process is not worth the effort since a full measurement sphere is required anyway. Also, unlike the SGH and FPA cases, when the NF data was acquired the DIP was pointed towards the poles of the measurement sphere, and the acquisition rules used here for demonstration purposes start at a pole (and hence at the minima of the DIP rather than the vicinity of the maxima), unlike the situation for the SGH and FPA.

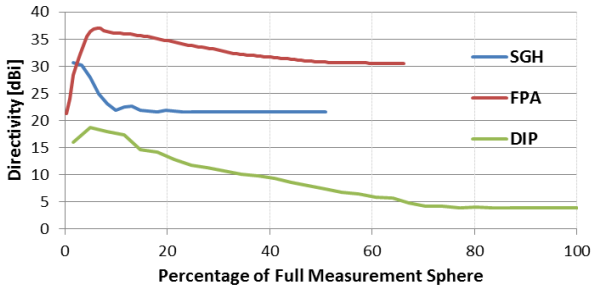

Figure 4 - Co-polarized directivity in the direction of maximum directivity (θ_0, ϕ_0) for each of the AUTs.

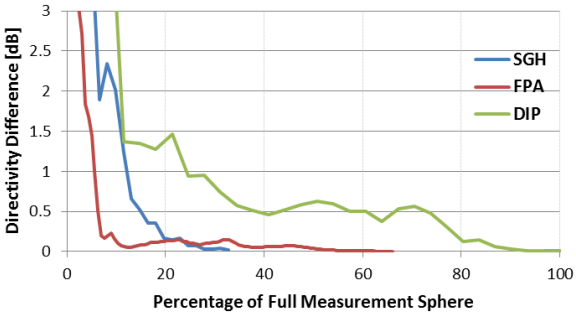

Figure 5 - Co-polarized directivity difference in the direction of maximum directivity (θ_0, ϕ_0) for each of the AUTs in Table 1.

5.2 Demonstration of the Acquisition Rule Examples

The first acquisition rule, as well as the second one with with a -5dB threshold level and iteration bands of width $\Delta\theta$ (m = 1), are used here with the SGH as the AUT. The results with the second and third decision functions are plotted in Fig.9 and Fig.10, respectively. In this case the two acquisition rules result in maps that would cause one to halt acquisition at the same stage. The reason is that the AUT has roughly the same principal plane beamwidths. If we were to test an AUT with an asymmetric type pattern, for example, there would be an advantage in using the "smarter" second acquisition rule as regards the map size at which acquisition is terminated. This is the subject of on-going investigation.

6. Concluding Remarks

An adaptive acquisition algorithm for SNF test time reduction has been proposed, and its feasibility demonstrated using selected acquisition rules and decision functions. It is possible to monitor the AUT performance measures while the testing is on-going and decide whether acquisition can be terminated after only sampling a percentage of the full measurement sphere. This directly implies that it will be possible to confidently reduce test time by similar percentages.

Studies of more comprehensive and refined sets of acquisition rules (eg. ones using field amplitude thresholds even in the second and subsequent iterations; ones that do not necessarily begin at the poles) and decision functions are underway to establish which might be best suited to test engineering practice. Other AUT types are being considered. We are also investigating of incorporating existing truncation error reduction methods into the adaptive algorithm.

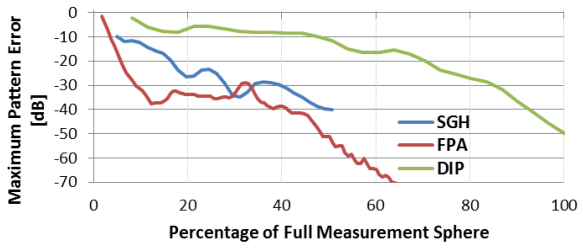

Figure 6 - Normalized co-polarized pattern error in the direction where this error is largest, for each of the AUTs in Table 1.

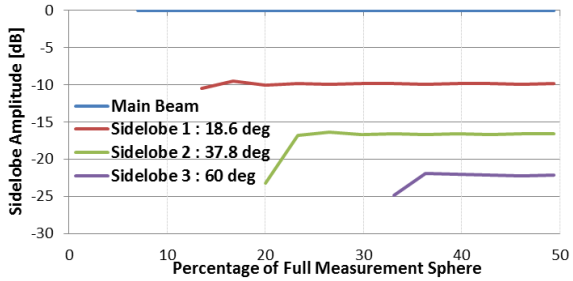

Figure 7 – Amplitude of the highest three sidelobes, relative to the radiation pattern maximum value, for the SGH as AUT.

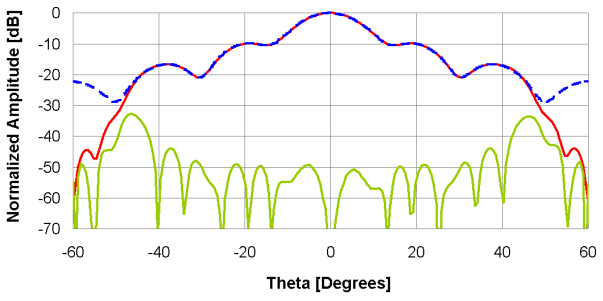

Figure 8 – Co-polarized radiation pattern of the SGH after eight iterations (——) of the adaptive SNF approach with the second acquisition rule, compared to that obtained from a full sphere acquisition (▪▪▪▪). The normalized error function is shown as (——).

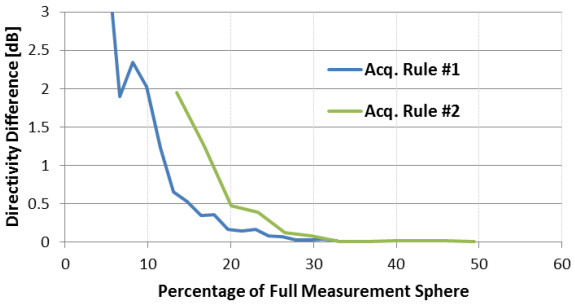

Figure 9 - Evolution of change in directivity for the two different acquisition rules, for the SGH as AUT, as the acquisition map increases.

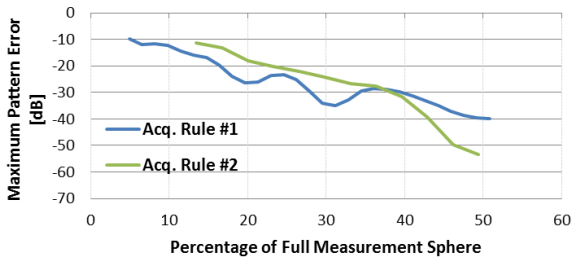

Figure 10 - Evolution of the normalized co-polarized pattern error (in the direction where this error is largest) for the two acquisition rules, with the SGH as AUT, as the acquisition map increases.

7. References

[1] D.J.Janse van Rensburg, D.A.McNamara & G.Parsons, "Adaptive acquisition techniques for planar near-field antenna measurements", Proc. *33rd Annual AMTA Symposium*, October 2011, Denver, USA.

[2] J.E.Hansen, *Spherical Near-field Antenna Measurements* (Peter Peregrinus Ltd, 1988).

[3] F.J.Cano-Facila and S. Pivnenko, "A new method to reduce truncation errors in partial spherical near-field measurements", Proc. *5th European Conf. Antennas Propagat.*, pp. 3259-3263, Rome, Italy, 2011.

[4] E.Martini, S.Maci and L.J.Foged, "Spherical near field measurements with truncated scan area", Proc. 5*th European Conf. Antennas Propagat.*, pp. 3256 - 3258, Rome, Italy, April 2011.

[5] Nearfield Systems Inc. (www.nearfield.com), USA.

[6] Mathworks (www.mathworks.com), USA